ACS Catalysis

Research Article

pubs.acs.org/acscatalysis

Screening Lewis Pair Moieties for Catalytic Hydrogenation of CO_2 in Functionalized UiO-66

Jingyun Ye[†] and J. Karl Johnson*[,†,‡]

[†]Department of Chemical & Petroleum Engineering, University of Pittsburgh, Pittsburgh, Pennsylvania 15261, United States

[‡]Pittsburgh Quantum Institute, Pittsburgh, Pennsylvania 15261, United States

Supporting Information

ABSTRACT: The capture and reuse of CO_2 as a liquid fuel could reduce the overall anthropogenic carbon footprint but requires a catalytic pathway for CO_2 hydrogenation under mild conditions, coupled with a renewable source of H_2 or another reducing agent. We have computationally designed eight functional groups having both Lewis acid and base sites for inclusion inside a porous metal−organic framework (MOF) and have evaluated these functionalized MOFs for their catalytic activity toward CO_2 hydrogenation. We have used density functional theory to compute reaction energies, barriers, and geometries for the elementary steps of CO_2 reduction. The reaction pathways involve two elementary steps for each of the eight functional groups, consisting of heterolytic dissociation of H_2 on the Lewis acid and base sites followed by concerted addition of a hydride and a proton to CO_2 in a single step. Our analysis of the reaction energetics reveals that the reaction barrier for hydrogen dissociation can be correlated as a function of the chemical hardness of the Lewis acid site. Furthermore, we have identified a Brønsted−Evans−Polanyi relationship relating the barrier for the second step, CO_2 hydrogenation, with the H_2 adsorption energy on the Lewis sites. Surprisingly, this linear relationship also holds for correlating the hydrogenation barrier with the hydride attachment energy for the gas-phase Lewis acid site. These correlations provide a computationally efficient method for screening functional groups for their catalytic activity toward CO_2 hydrogenation. These relationships are further utilized to carry out a Sabatier analysis on a simplified model of the reaction to generate contour plots of the Sabatier activity that can be used to identify properties of the functional groups for maximizing the reaction rate.

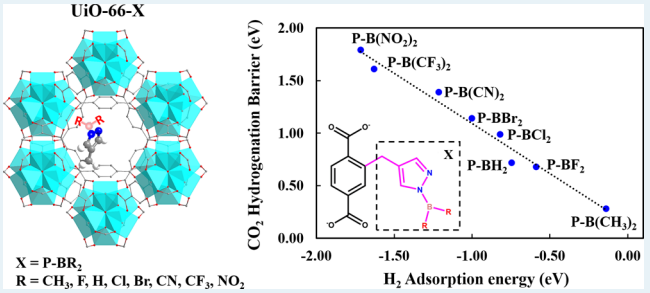

KEYWORDS: *Lewis acid, Lewis base, density functional theory, carbon dioxide hydrogenation, CO_2 utilization, formic acid synthesis, Brønsted−Evans−Polanyi relationship, Sabatier activity*

1. INTRODUCTION

The widespread use of fossil fuels generates enormous quantities of CO_2, leading to increasing concentrations of this greenhouse gas in the atmosphere, which has been linked to global warming.[1] The use of fossil fuels is likely to continue over the next several decades as renewable energy sources gradually become more prevalent, making CO_2 capture coupled with sequestration or utilization an important near-term approach for reducing CO_2 emissions.[2−5] Interest in using CO_2 as a feedstock for the synthesis of valuable products has grown in recent years as a supplement or alternative to sequestration.[1,6−8] Specifically, catalytic hydrogenation of CO_2 is a promising means of producing high-energy-density fuels from CO_2 captured from combustion waste streams.[6,7,9−16] In this paper we use density functional theory as a tool for screening and characterizing a series of catalysts for reduction of CO_2 to formic acid (FA) with H_2. In practice, we envision generation of H_2 from renewable but intermittent energy sources, such as wind or solar, thus coupling energy storage with CO_2 mitigation through an anthropogenic chemical carbon cycle.[7,17] Hydrogenation of CO_2 to FA can be viewed as the first step in the production of methanol or other hydrogenated species, but it is also a commercially valuable product in its own right.[18−21]

Hydrogenation of CO_2 to FA via homogeneous catalysis has been extensively studied in the past.[8,14,22−27] The main advantage of the homogeneous route to CO_2 reduction is that the reaction can be carried out under relatively mild conditions in comparison with most heterogeneous catalytic routes.[15,27,28] The major challenges to homogeneous catalysis are efficient capture and recycling of the precious-metal catalysts,[8,28,29] limited liquid-phase solubility of H_2 gas, which leads to significant mass transfer limitations,[14] and economical regeneration of FA from the salts used to separate it from the solution and shift the equilibrium conversion.[8,30] An ideal catalyst for large-scale industrial CO_2 hydrogenation would combine the advantages of homogeneous and heterogeneous

Received: June 8, 2015
Revised: September 7, 2015
Published: September 14, 2015

DOI: 10.1021/acscatal.5b01191
ACS Catal. 2015, 5, 6219−6229

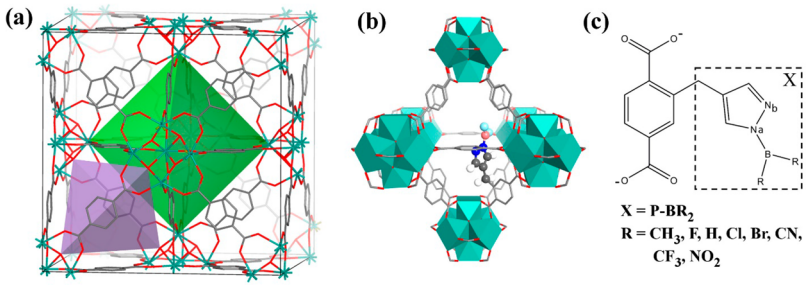

Figure 1. Lewis pair functionalized UiO-66 (UiO-66-X). (a) Octahedral cage (green) and tetrahedral cage (purple) of the unit cell of UiO-66. (b) LP functionalized BDC ligand of the octahedral cage of UiO-66. The UiO-66 framework atoms are represented by lines, and the Lewis pair functional moieties are represented by balls and sticks. Atom colors: gray for C, red for O, blue for N, pink for B, cyan polyhedra for Zr, light blue for F. Hydrogen atoms belonging to the framework are not shown for clarity. (c) Lewis pair functional groups X used in this work, where X is P-$B(CH_3)_2$, P-BF_2, P-BH_2, P-BCl_2, P-BBr_2, P-$B(CN)_2$, P-$B(CF_3)_2$, and P-$B(NO_2)_2$ (P denotes the 4-methylpyrazole group). The boron atom (B) is the Lewis acid site, and the nitrogen labeled N_b is the Lewis base site. The other nitrogen is labeled N_a for later reference.

catalysts.[9,26] The overall goal of our work is to provide the insight needed to design such a catalyst.

Our approach to designing a CO_2 hydrogenation catalyst is to use computational tools to identify homogeneous-like catalytic moieties that can be covalently bound inside porous metal organic framework (MOF) materials and to estimate their activities by using density functional theory (DFT) to compute reaction energies and barriers. Our hypothesis is that we can create molecular catalysts that will be active when bound to the inside of the pores of MOFs and that these catalytically functionalized MOFs will exhibit the advantages of both homogeneous and heterogeneous catalysts.[31−35] We have shown in previous work[36] that this approach will work in principle by attaching a functional group to the 1,4-benzenedicarboxylate (BDC) linker in a highly stable and functionalizable MOF known as UiO-66.[37,38] We have shown from DFT calculations that this functionalized UiO-66 is catalytically active for CO_2 hydrogenation and that the reaction can be carried out in the absence of a solvent by exposing the functionalized MOF to gas streams of H_2 and CO_2.[36] However, identifying a single catalyst does not provide much information on how to develop an optimal catalyst. Computational methods are becoming ever more useful tools in the quest for rational catalyst design.[39−42] Specifically, Brønsted−Evans−Polanyi (BEP) relationships[43,44] and scaling properties[45] have been tremendously fruitful approaches for providing insight into the rational design of metallic catalysts.[39,42,45−54] In this paper we seek to apply BEP relationships and other correlations to functionalized UiO-66 in order to provide the insight needed to design more active catalysts and rapidly screen various functional groups for CO_2 hydrogenation, identifying the most promising materials for either detailed DFT calculations or experimental investigation.

We examine a series of eight different functional groups, each incorporated into UiO-66 as shown in Figure 1. The UiO-66 unit cell is shown in Figure 1a and has both larger octahedral cages and smaller tetrahedral cages connected by triangular windows, making a three-dimesnsional porous network. A functional group in the octahedral cage attached to one of the BDC linkers is shown in Figure 1b. All of the functional groups considered in this work are composed of Lewis pairs (LPs): that is, moieties having both Lewis acid and base sites. The functional groups are attached to one of the BDC linkers in the UiO-66 primitive cell, as shown in Figure 1c. Each LP functional group examined here is based on 1-(difluoroboranyl)-4-methylpyrazole, denoted as P-BF_2, which we designed in our previous work for hydrogenation of CO_2.[36] We change the R groups on the boron atom shown in Figure 1c in order to generate the eight different LP moieties.

Our choice of LP functional groups in this work was inspired by the use of frustrated Lewis pairs (FLPs) as catalysts for CO_2 hydrogenation[55−64] and by their ability to both bind CO_2 and heterolytically dissociate H_2 without the use of precious metals.[65−69] However, to the best of our knowledge there are only two examples of FLPs being used to reduce CO_2 with H_2.[63,64] All other studies use reducing agents such hydroboranes that are not readily reversible and so do not provide a sustainable pathway for CO_2 reduction. In addition, FLPs are homogeneous catalysts and therefore are not as useful for large-scale industrial processes as heterogeneous catalysts. We note that the LP moieties in our work do not require steric hindrance to prevent mutual quenching as is the case for FLPs because they are covalently bound to the UiO-66 framework through the BDC linkers and are not mobile.

The goals of this work are to (1) test a number of possible LP functional groups for their activity toward CO_2 hydrogenation, (2) identify approximate relationships that will facilitate rapid screening of functional groups, and (3) identify general features that influence the reaction barriers for CO_2 reduction, leading to principles that we hope will allow for the rational design of better catalysts. To achieve this last goal, we have developed BEP relationships[43,44] and other correlations of reaction enthalpies and barriers with chemical descriptors such as acidity, basicity, and electrostatics and geometric parameters such as acceptor−donor distances and bonding angles.[70−81] These relationships are utilized to develop a simple Sabatier analysis[82] to identify properties of the functional groups that lead to maximum reaction rates.

2. COMPUTATIONAL DETAILS

All periodic DFT calculations were performed in the mixed Gaussian plane wave scheme as implemented in CP2K.[83] van der Waals interactions were approximated with the D3 dispersion correction developed by Grimme et al.[84] The Perdew−Burke−Ernzerhof (PBE) functional[85] was used to calculate the exchange correlation energy. The DZVP-MOLOPT basis set in combination with Geodecker, Teter, and Hutter pseudopotentials[86] were used for the atomic species, with a plane wave cutoff energy of 360 Ry and a relative cutoff of 60 Ry. These values were tested previously and were shown to give converged energies for functionalized UiO-66.[36]

DOI: 10.1021/acscatal.5b01191
ACS Catal. 2015, 5, 6219−6229

The adsorption (chemisorption) energy of CO_2 or H_2 is defined as

$$E_{ad}(M) = E(M/UiO\text{-}66\text{-}X) - E(UiO\text{-}66\text{-}X) - E(M) \quad (1)$$

where M represents CO_2 or H_2, UiO-66-X represents UiO-66 functionalized with one of the eight functional groups denoted by X, and E(M/UiO-66-X), E(UiO-66-X), and E(M) represent the total energy of UiO-66-X with the adsorbate, empty UiO-66-X, and the gas-phase molecule M, respectively. In the case of coadsorption, the adsorption energies were computed with respect to the sum of the total energies of the corresponding gas-phase molecular species. According to the definition above, negative values indicate that the process is exothermic and positive values are endothermic.

Transition states along the reaction pathway were determined by using the climbing image nudged elastic band (CI-NEB) method[87] and were further confirmed through frequency analysis. Transition states were found to have a single imaginary frequency for a vibrational mode aligned with the reaction trajectory.

We have calculated selected molecular properties of the isolated (gas-phase) LP molecules, denoted as X, and LP radicals, meaning that we leave the CH_2 group that binds the moiety to the linker (shown in Figure 1c) unsaturated. This unsaturated LP radical is denoted as -X. Thus, X denotes the LP molecule having CH_3 on the 4-position of the pyrazole ring and -X indicates a CH_2 radical at the 4-pyrazole position. We computed adsorption (reaction) energies for both CO_2 and H_2, the acidity and basicity for each of the eight LP molecules, and the electronegativity, hardness, and softness for each of the eight LP radicals. The Gaussian09 program[88] was used for these gas-phase cluster calculations. The hybrid density functional method M06-2X[89] combined with the 6-311++g(d,p) basis set was used for all these calculations. We used the M06-2X functional for cluster calculations because it has been shown to be more accurate than pure density functionals[89] and has been previously used for computing molecular properties of FLPs.[90]

We have used the hydride and proton attachment energies as measures of the acidity and basicity of the LPs, respectively, as has been done for FLPs.[70] The hydride attachment energy is defined as

$$\Delta G_{ha} = G([XH]^-) - G(X) - G([H]^-) \quad (2)$$

and the proton attachment energy is computed from

$$\Delta G_{pa} = G([XH]^+) - G(X) - G([H]^+) \quad (3)$$

where G(X), $G([H]^-)$, $G([H]^+)$, $G([XH]^-)$, and $G([XH]^+)$ represent the Gibbs free energies of the LP X, the hydride, the proton, the hydride attached to the LP ($[XH]^-$), and the protonated LP ($[XH]^+$), respectively. ΔG_{ha} and ΔG_{pa} represent the changes in the Gibbs free energy for hydride attachment and proton attachment in the gas phase, respectively. More negative ΔG_{ha} values indicate stronger acidity, and more negative ΔG_{pa} values correspond to stronger basicity. Note that we use the gas phase instead of an implicit or explicit solvent because we are relating these quantities to reactions within the functionalized MOFs, which occur by gas-phase adsorption of H_2 and CO_2 into the pores of the MOF. Hence, the reaction environment in the MOF probably more closely reflects a gas-phase than a solution-phase environment. Additionally, we have carried out test calculations using an implicit solvent model to assess the impact of solvent effects on the results. These calculations showed the same trends between the gas-phase and implicit solvent calculations (see Table S1 in the Supporting Information), indicating that correlations relating acidities and basicities to adsorption energies will work equally well for gas-phase or implicit solvent calculations.

We have calculated the electronegativity (χ), hardness (η), and softness (S) for each of the gas-phase LP radicals. We follow the approach of reported by Geerlings et al.[91] of computing the ionization energy and electron affinity on the neutral LP radical. That is, we fix the geometry of the LP as it is bound to the BDC linker in UiO-66-X but keep the terminal group CH_2 unsaturated. We have used the Mulliken formula[92] to compute χ, which Parr et al.[93] identified as a finite difference approximation

$$\chi = -\mu = -\left(\frac{\partial E}{\partial N}\right)_{v(r)} \approx \left(\frac{I + A}{2}\right) \quad (4)$$

where μ and $v(r)$ denote the chemical and external potentials, respectively, E represents the electronic total energy, N is the number of electrons, I is the ionization potential, and A is the electron affinity of the molecule.

The chemical hardness and its finite difference formula were defined by Parr and Pearson as[94]

$$\eta = \frac{1}{2}\left(\frac{\partial^2 E}{\partial^2 N}\right)_{v(r)} \approx \left(\frac{I - A}{2}\right) \quad (5)$$

The softness is given by

$$S = \left(\frac{1}{I - A}\right) \quad (6)$$

3. RESULTS AND DISCUSSION

3.1. Synthesis and Stability of Functionalized MOFs. There are a wide range of options available for functionalizing UiO-66.[34,95−105] We have addressed the issue of how one might specifically synthesize UiO-66-P-BF_2 in a previous paper.[36] Similar approaches could be used to synthesize the other MOFs identified in this work.

One indirect indication of the stability of a functionalized MOF is how much the framework is perturbed upon functionalization.[36] As a test of the stability of the different functional groups explored in this work, we have computed the lattice distortions of the largest functional group, P-B$(CF_3)_2$. The fully relaxed cell parameters of UiO-66-P-B$(CF_3)_2$ are $a = b = c = 14.790$ Å and $\alpha = \beta = \gamma = 60°$. These values are almost identical with the relaxed UiO-66 values of $a = b = c = 14.788$ Å and the same angles. This indicates that even for the largest functional group considered in this work the lattice structure is essentially unchanged. We therefore expect the thermodynamic stability of any of the UiO-66-X materials to be very similar to that of unfunctionalized UiO-66.

3.2. H_2 and CO_2 Adsorption in UiO-66-X. In this study we compute the thermodynamics and reaction pathways for a family of LP functionalized UiO-66 systems, denoted as UiO-66-X, where X = P-B$(CH_3)_2$, P-BF_2, P-BH_2, P-BCl_2, P-BBr_2, P-B$(CN)_2$, P-B$(CF_3)_2$, P-B$(NO_2)_2$. The structures of these materials are shown in Figure S1 of the Supporting Information.

One of the key advantages of using functionalized MOFs is that the reactions can be carried out by exposing the porous catalysts to gas-phase H_2 and CO_2 rather than using a solution-

DOI: 10.1021/acscatal.5b01191
ACS Catal. 2015, 5, 6219−6229

phase reaction mechanism required for homogeneous reactions. The initial step of the reaction mechanism is the adsorption of H_2 or CO_2 from the gas phase. We have not explicitly simulated this first step because there are experimental papers demonstrating that both of these gases can readily adsorb in UiO-66 and its functional derivatives.[95,106−111] These experimental results indicate that adsorption of H_2 and CO_2 is both thermodynamically and kinetically favored near room temperature (and also at 77 K for H_2), notwithstanding the entropic penalty for these gases to adsorb into a microporous material. Thus, we focus our efforts on computing the reaction energies and barriers assuming that the guest molecules can be readily introduced into the pores.

We have computed the adsorption (reaction) energies of H_2 and CO_2 in UiO-66-X. These adsorption energies correspond to the enthalpies of reaction at 0 K for H_2 heterolytic dissociation of H_2 or for CO_2 chemisorption; the values are given in Figure 2, the structures are shown in Figures S2 and S3 of the Supporting Information, and selected structural details (bond lengths and angles) are given in Table S2 of the Supporting Information. The adsorption mechanism of H_2 in UiO-66-X is the same for each functional group X: H_2 heterolytically dissociates with one H atom bound to B and another H atom bound to the nitrogen denoted N_b, as shown in Figure 2a, where N_b is identified as the Lewis base site as shown in Figure 1c, generating hydridic and protic hydrogens, respectively (see Figure S2 for the structures of dissociated H_2 on UiO-66-X). The magnitude of the dissociative adsorption energy for H_2 in UiO-66-X increases as P-B$(CH_3)_2$ < P-BF_2 < P-BH_2 < P-BCl_2 < P-BBr_2 < P-B$(CN)_2$ < P-B$(CF_3)_2$ < P-B$(NO_2)_2$, as can be seen in Figure 2.

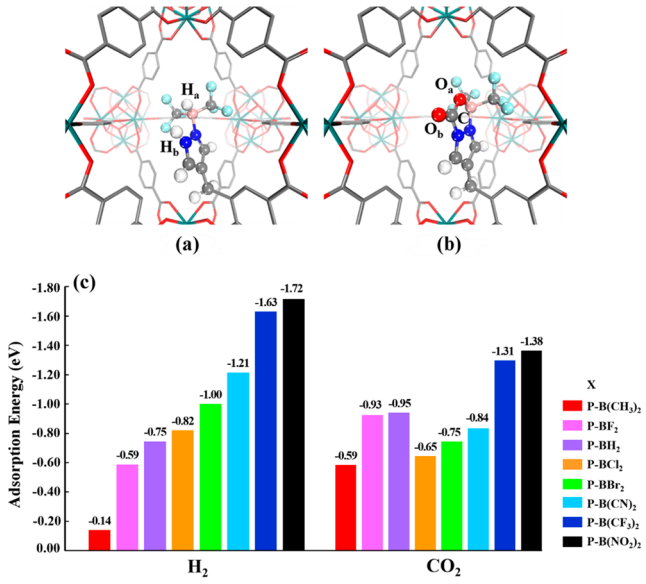

Figure 2. Structures of (a) H_2 and (b) CO_2 chemisorbed in UiO-66-P-B$(CF_3)_2$ and (c) the calculated adsorption energies (0 K, no zero-point energy corrections) of H_2 and CO_2 in UiO-66-X.

CO_2 is chemically adsorbed in each UiO-66-X in a bent structure with one O atom bound to B and the C atom bound to N_b, as shown in Figure 2b (see Figure S3 in the Supporting Information). The trend in adsorption energies for CO_2 in UiO-66-X follows the same general trend as the H_2 adsorption energies, except that P-BF_2 and P-BH_2 are out of sequence, having larger adsorption energies than the next three groups in the sequence, as can be seen from Figure 2. The adsorption energies for H_2 and CO_2 are fairly similar for most of the functional groups; five of the functional groups adsorb H_2 more strongly, and three adsorb CO_2 more strongly. Our calculations indicate that H_2 and CO_2 will bind competitively to these groups, except for P-B$(CH_3)_2$, for which the H_2 adsorption energy is very weak.

3.3. CO_2 Hydrogenation in UiO-66-X. Our previous work identified the reaction mechanism for HCOOH production from CO_2 hydrogenation in UiO-66-P-BF_2 as consisting of two steps: (1) heterolytic H_2 dissociation on the LP moiety (H_2(vdW) → 2H*) followed by (2) concerted addition of the hydridic hydrogen to C and the protic hydrogen to O on CO_2 that is physically adsorbed in the pore (CO_2 + 2H* → HCOOH).[36] The concerted two-electron reduction via simultaneous addition of a hydridic and protic species proceeds via a lower energy pathway in comparison to sequential one-electron reductions, as shown by Zimmerman et al. in the case of CO_2 reduction by ammonia−borane.[112] In this work we show that the reaction mechanisms for CO_2 hydrogenation for each of the seven other UiO-66-X catalysts follow the same two-step mechanism. The potential energy profiles are shown in Figure 3, and the forward and reverse reaction barriers for the two elementary steps are reported in Table 1 (the relative energies for Figure 3 are given in Table S3 of the Supporting Information). Figure 3 and Table 1 report the 0 K energies without zero-point vibrational energy (ZPE) corrections. Structural details and CI-NEB pathway energetics for the reactions are given in Figures S4−S10 and Tables S4 and S5 of the Supporting Information.

Molecular hydrogen physisorbs in the porous framework, forming a van der Waals complex H_2(vdW) prior to H_2 dissociation. The energies of the H_2(vdW) complexes in the different UiO-66-X materials fall in a narrow range of −0.08 to −0.17 eV. The energies for H_2 dissociation in UiO-66-X (TS1 in Figure 3) increase as follows: P-BF_2 < P-B$(CF_3)_2$ < P-BH_2 < P-BBr_2 < P-BCl_2 < P-B$(NO_2)_2$ < P-B$(CN)_2$ < P-B$(CH_3)_2$. The dissociation barriers range from 0.48 to 1.09 eV. The reaction barriers for H_2 dissociation, E_f, are lower than the backward barriers for H_2 formation, E_b, for all functional groups except UiO-66-P-B$(CH_3)_2$, for which E_f and E_b are about the same. Therefore, H_2 dissociation is both thermodynamically and kinetically more favorable than the backward reaction in all UiO-66-X species except UiO-66-P-B$(CH_3)_2$.

The second elementary step proceeds as CO_2 is physisorbed in UiO-66-X occupied by dissociated H atoms, which we denote CO_2 + 2H* in Figure 3. The CO_2 adsorption energies (difference between the energies of CO_2 + 2H* and 2H* in Figure 3) range from −0.26 to −0.42 eV, indicating that the physorption of CO_2 in UiO-66-X with dissociated H atoms is energetically favorable. The energy barriers for CO_2 hydrogenation in UiO-66-X increase as follows: P-B$(CH_3)_2$ < P-BF_2 < P-BH_2 < P-BCl_2 < P-BBr_2 < P-B$(CN)_2$ < P-B$(CF_3)_2$ < P-B$(NO_2)_2$. This ordering is same as the dissociative adsorption energies for H_2 in UiO-66-X (see Figure 2). The backward reaction barriers for FA dissociation (HCOOH → CO_2 + 2H*) in UiO-66-X range from 0.35 to 0.64 eV; these values are lower than the forward reaction barriers in all cases except for UiO-66-P-B$(CH_3)_2$. However, diffusion of FA through the pores of UiO-66 is facile, having a diffusion barrier of only about 0.07 eV according to our calculations (see Figure S11 in the Supporting Information), so that FA may diffuse away from the catalyst site and desorb into the gas phase rather than follow the backward

DOI: 10.1021/acscatal.5b01191
ACS Catal. 2015, 5, 6219−6229

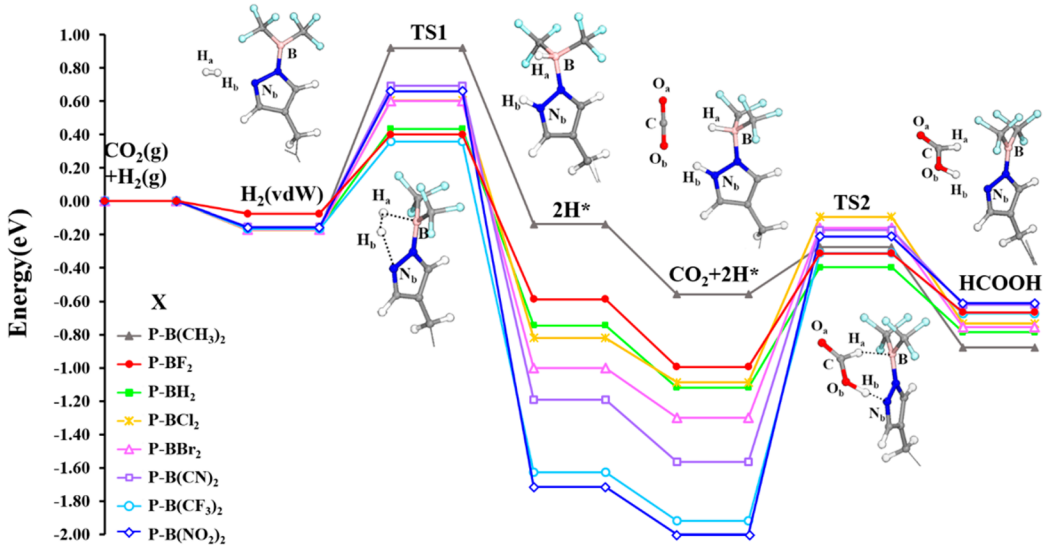

Figure 3. Potential energy profiles (0 K, no ZPE corrections) for CO_2 hydrogenation in UiO-66-X. The gas-phase (desorbed) *trans*-FA has an energy of −0.20 eV on this scale. Key structures are shown in the diagram for the P-B$(CF_3)_2$ functional group as examples.

Table 1. Forward (E_f) and Backward (E_b) Reaction Barriers for H_2 Dissociation (Step 1) and CO_2 Hydrogenation (Step 2) in UiO-66-X[a]

	step 1		step 2	
UiO-66-X	E_f (eV)	E_b (eV)	E_f (eV)	E_b (eV)
UiO-66-P-B$(CH_3)_2$	1.09	1.06	0.28	0.60
UiO-66-P-BF_2	0.48	0.99	0.68	0.35
UiO-66-P-BH_2	0.59	1.18	0.72	0.39
UiO-66-P-BCl_2	0.78	1.43	0.99	0.64
UiO-66-P-BBr_2	0.77	1.60	1.14	0.60
UiO-66-P-B$(CN)_2$	0.84	1.88	1.39	0.45
UiO-66-P-B$(CF_3)_2$	0.53	1.85	1.61	0.36
UiO-66-P-B$(NO_2)_2$	0.82	2.38	1.79	0.40

[a]The energies are given at 0 K, with no ZPE corrections.

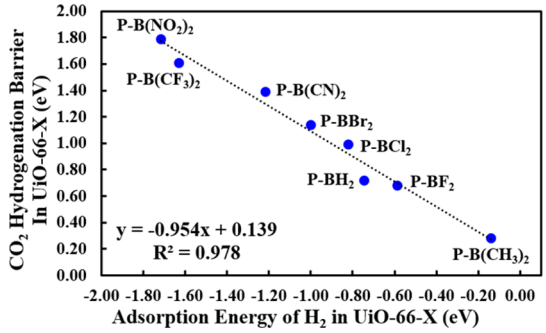

Figure 4. Calculated reaction energy barriers for CO_2 hydrogenation in UiO-66-X (step 2 in Table 1) as a function of the adsorption energies of H_2 in UiO-66-X.

reaction as long as the external concentration of FA is kept low. Note that *cis*-FA is produced in the pore from the reactions given in Figure 3, whereas *trans*-FA is the lowest energy confirmer in the gas phase. However, our calculations indicate that *cis*-FA is actually lower in energy than *trans*-FA in the pore because of confinement effects, which is opposite from the situation in the gas phase (see Figure S12 in the Supporting Information). Our calculated gas-phase *trans*-FA energy (0 K, not ZPE corrected) is 0.20 eV lower than those for gas-phase H_2 and CO_2 ; thus, gas-phase *trans*-FA is 0.4−0.5 eV higher in energy than the adsorbed *cis*-FA product state shown in Figure 3. However, desorption is entropically favored. Note that our 0 K energies indicate that the reaction of CO_2 with H_2 to form FA is exothermic by 0.2 eV, whereas at 298 K the reaction is endothermic by about 0.15 eV. The difference in the reaction energies can be ascribed to the difference in temperatures and the approximate nature of the DFT functionals.

3.4. Trends in CO_2 Hydrogenation Barriers. As noted above, CO_2 hydrogenation barriers follow the same trend as the H_2 adsorption energies. Indeed, a plot of the barriers as a function of the adsorption energies for each of the functional groups gives an essentially linear BEP relationship, as shown in Figure 4. A fit to the data gives a coefficient of determination of $R^2 = 0.978$. The BEP relationship can be rationalized by noting that weakly bound H atoms at the Lewis acid and base sites more readily bind to CO_2 in the hydrogenation reaction, whereas strongly bound H atoms require more energy to break the stronger bonds with the Lewis sites. The correlation shown in Figure 4 indicates that the reaction barriers for CO_2 hydrogenation in UiO-66-X can be estimated fairly accurately from the reaction energies for H_2 dissociation in UiO-66-X, which are much easier to compute than the barriers. This gives us a useful tool for screening different LP functional groups.

Notwithstanding that the adsorption energies for H_2 in UiO-66-X are much less computationally demanding to obtain than the transition states, they are still relatively expensive to calculate in comparison with adsorption energies on the isolated (gas phase) LPs because of the large number of UiO-66 framework atoms included in the former calculation. We therefore computed the adsorption energies of H_2 on the gas-phase LPs to see if these values could be used as surrogates for the values computed for the full periodic system. The gas-phase adsorption energies for H_2 and CO_2 on the functional groups are given in Tables S6 and S7, respectively, in the Supporting Information. The adsorption energies for H_2 on the gas-phase moieties and the full UiO-66-X structures are plotted in Figure 5. We observe a quantitative linear correlation between the two calculations, which indicates the existence of a BEP relationship between the gas-phase H_2 adsorption energies

DOI: 10.1021/acscatal.5b01191
ACS Catal. 2015, 5, 6219−6229

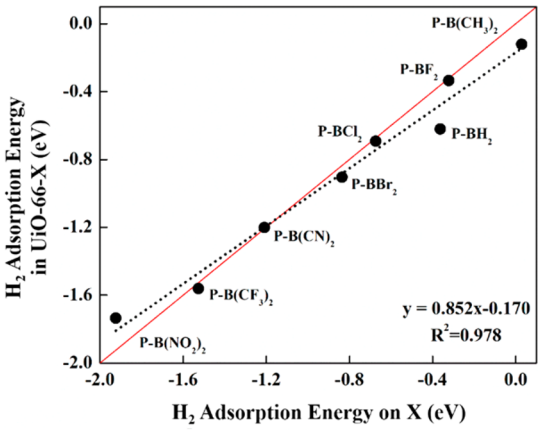

Figure 5. Adsorption energies of H_2 in UiO-66-X plotted as a function of the H_2 adsorption energies on the gas-phase Lewis pairs, X. The solid red line is the $y = x$ line denoting a perfect correspondence between the two quantities. The dashed line is a linear fit to the adsorption energy in UiO-66-X as a function of the gas-phase Lewis pair, X.

on the LPs and the CO_2 hydrogenation energy barriers in UiO-66-X.

A plot of the reaction barriers for CO_2 hydrogenation in UiO-66-X as a function of the gas-phase adsorption energies of H_2 on the LPs (Figure 6) confirms that the BEP relationship

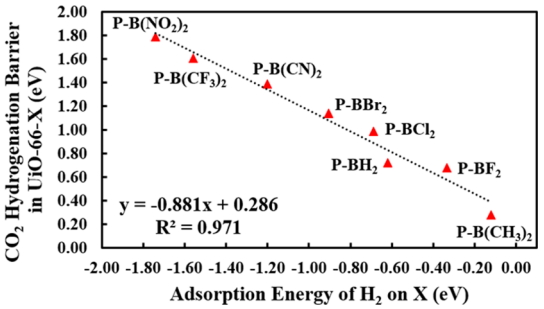

Figure 6. Calculated reaction barrier energies for CO_2 hydrogenation in UiO-66-X (step 2 in Table 1) plotted as a function of the adsorption energy of H_2 on the gas-phase Lewis pair, X.

holds with almost the same goodness of fit, $R^2 = 0.971$. This observation provides a very efficient method for screening functional groups. The relatively quick calculation of the H_2 adsorption energy on a gas-phase LP can be used to rapidly estimate the reaction barrier for CO_2 hydrogenation in LP functionalized UiO-66. However, this BEP relationship is not sufficient to estimate the activity of the proposed catalyst because the barrier for H_2 dissociation may be similar to the CO_2 hydrogenation barrier (see Table 1). Hence, there is a need for a method to estimate the H_2 dissociation barriers. This will be addressed in section 3.6.

3.5. Role of Acidity in H_2 Adsorption. The dissociative adsorption energy of H_2 on the LP sites should be influenced by the acidity and basicity of LPs, as has been demonstrated for FLPs.[70] We have computed the proton and hydride attachment free energies as measures of the basicity and acidity, respectively, for all eight LPs; the values are given in Table 2. The proton attachment energies (ΔG_{pa}) are found to lie in a comparatively narrow range. This is because the substitutional groups that differentiate each LP are all attached to the boron

Table 2. Free Energies of Proton Attachment (Basicity) and Hydride Attachment (Acidity) of the Lewis Pairs X in the Gas Phase

X	ΔG_{pa} (eV)	ΔG_{ha} (eV)
P-B$(CH_3)_2$	−9.57	−2.61
P-BF_2	−9.07	−3.21
P-BH_2	−9.25	−2.95
P-BCl_2	−9.16	−3.89
P-BBr_2	−9.19	−4.22
P-B$(CN)_2$	−8.60	−4.78
P-B$(CF_3)_2$	−8.70	−4.96
P-B$(NO_2)_2$	−9.12	−5.59

acid site and have little effect on the basicity of each group. Thus, there is no correlation between ΔG_{pa} and the H_2 adsorption energies. In contrast, the hydride attachment energies (ΔG_{ha}) correlate very well with H_2 adsorption energies on the gas-phase LPs, as shown in Figure 7a. More importantly, the correlation is also valid for H_2 adsorption energies for the functional groups bound inside frameworks, as seen in Figure 7b, where we plot the H_2 adsorption energies in UiO-66-X as a function of ΔG_{ha} for each gas-phase LP, X. The correlations between ΔG_{ha} and the adsorption energies can be combined with the results of Figures 4 and 6 to develop a linear scaling relationship between ΔG_{ha} and the CO_2 hydrogenation barrier; this relationship is shown in Figure 7c. This figure illustrates the simple rule of thumb that the stronger the acid site in the LP, the stronger the H_2 binding energy and hence the higher the reaction barrier for CO_2 hydrogenation. Therefore, the hydride attachment energy could be used to screen candidate LPs for CO_2 hydrogenation. Moreover, reduction of the Lewis acidity for LPs should lead to an increase in the activity of UiO-66-X for CO_2 hydrogenation. However, we note that one must also consider the barrier for H_2 dissociation, which does not scale with acidity (vide infra), in the overall activity of the material. This again highlights the need to develop a descriptor for the H_2 dissociation barrier.

3.6. Correlating the H_2 Dissociation Barrier. We have investigated multiple properties of the LP functional groups in a search to identify a descriptor for the H_2 dissociation barrier. We have considered the acidity, basicity, electronegativity, hardness, and softness of the gas-phase LP groups (these last three properties are reported in Table S8 of the Supporting Information). We also examined the structural details of the LP functional groups inside UiO-66-X, with and without dissociated H_2 (Tables S9 and S10 in the Supporting Information), and the charges on the acid and base sites (Table S11 in the Supporting Information). Of these properties, we found that only the hardness of the LP radicals, as computed from eq 5, and the N_b−N_a−B bond angle (without dissociated H_2) give meaningful correlations with the H_2 dissociation barriers. The barrier for H_2 dissociation in UiO-66-X scales roughly linearly with the hardness of the LP radicals, -X, as shown in Figure 8a. We note that, since all the functional groups contain the same Lewis base (N_b), the reaction barrier is dependent on the hardness of the Lewis acid (B), which is modulated by the different substituent R groups (Figure 1c). Increasing the hardness of the Lewis acid site should increase the activity of UiO-66-X for H_2 dissociation, which follows the principle that hard acids react more readily with hard bases or soft acids, such as H_2.[113,114]

DOI: 10.1021/acscatal.5b01191
ACS Catal. 2015, 5, 6219−6229

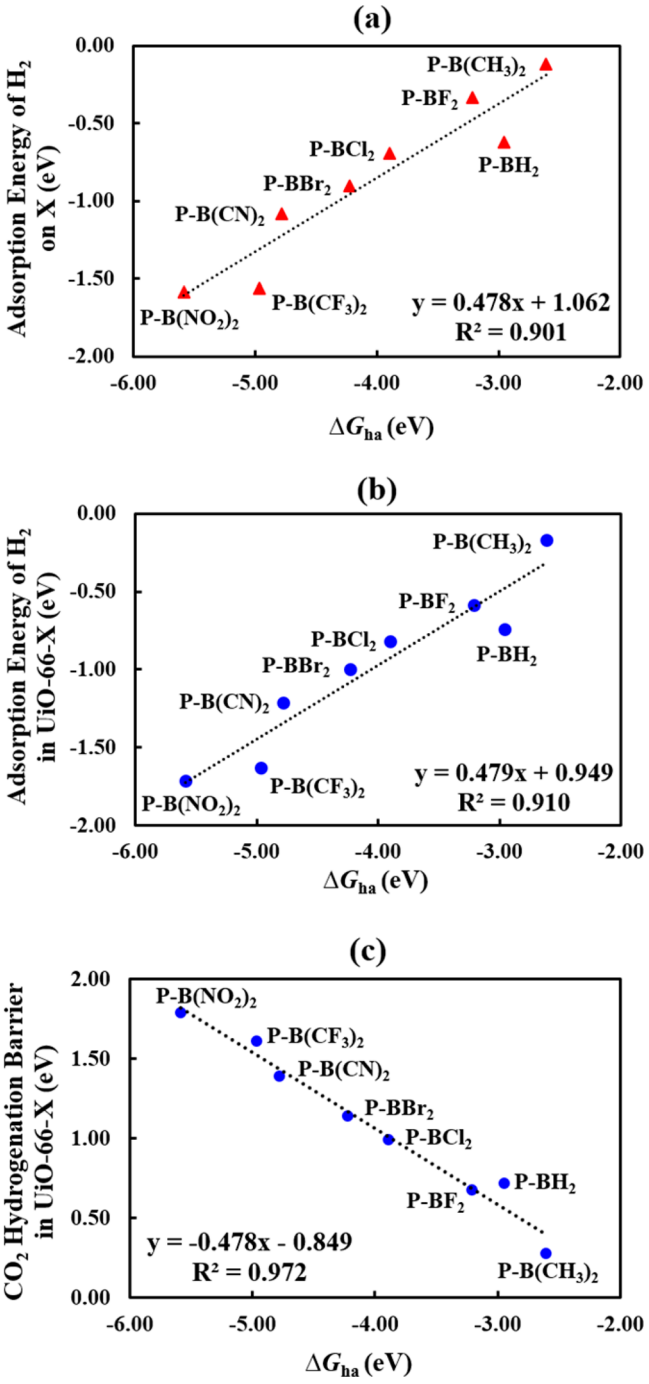

Figure 7. Calculated adsorption energies for H_2 (a) on the gas-phase Lewis pair X and (b) in UiO-66-X plotted as a function of hydride attachment energy (ΔG_{ha}) for the Lewis pair X. (c) Calculated reaction barrier energies for CO_2 hydrogenation in UiO-66-X versus ΔG_{ha}.

We also found that the barrier for H_2 dissociation in UiO-66-X is, to a good approximation, a linear function of the bond angle of the electron acceptor−donor moiety ($\angle N_b{-}N_a{-}B$), as can be seen in Figure 8b. This result can be rationalized by noting that a larger angle produces strain in the LP, which lowers the reaction barrier for H_2 dissociation. We see that the H_2 dissociation barriers for UiO-66-$B(CH_3)_2$ and UiO-66-$B(CF_3)_2$ do not fit the trend lines in Figure 8; these are shown as triangles in the graphs and were excluded from the fitting of

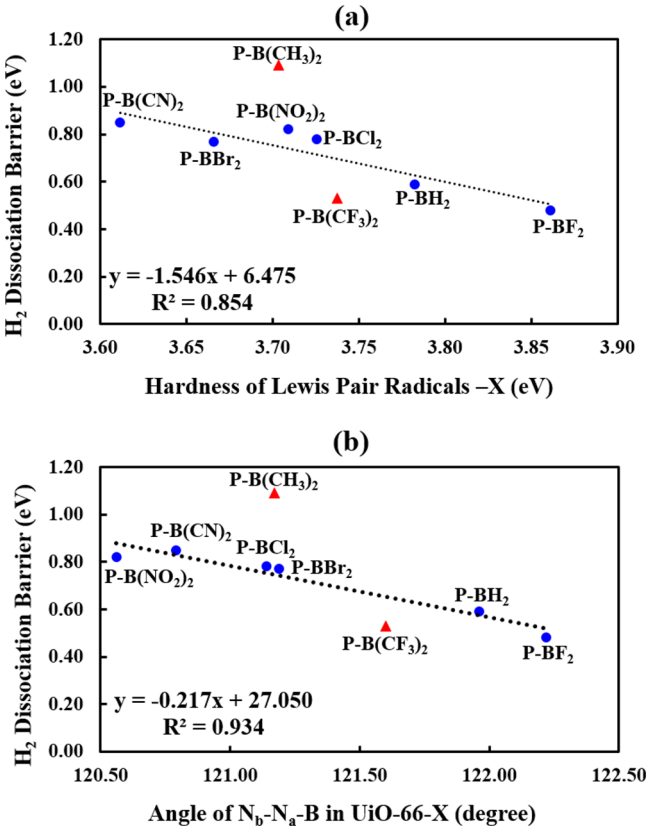

Figure 8. Calculated barriers for H_2 dissociation in UiO-66-X plotted as a function of (a) the hardness of Lewis pair functional groups (-X) and (b) the electron acceptor−donor bond angle ($\angle N_b{-}N_a{-}B$) in UiO-66-X.

the trend lines. We were unable to conclusively identify reasons for these two functional groups not following the trends.

We have identified a BEP relationship between the barriers for the reverse reaction ($2H^* \rightarrow H_2(vdW)$) and the adsorption energies of H_2 in UiO-66-X, as shown in Figure S13a of the Supporting Information. Furthermore, the barriers for H_2 formation in UiO-66-X scale linearly with the hydride attachment energies of each Lewis pair X, which indicates that a reduction of the acidity of the Lewis pair will lower the barrier for H_2 liberation. This result is in good agreement with a similar observation for FLPs.[79]

3.7. Model for the Sabatier Activity. The BEP relationships for the H_2 dissociation and CO_2 hydrogenation barriers and the correlations for the H_2 adsorption energies can be combined with a very simple microkinetic model to identify optimum properties of the LP functional groups through a Sabatier analysis.[39,47,50,115] In order to simplify the system to arrive at a 2-dimensional Sabatier analysis, we assume that adsorption of H_2 and CO_2 from the gas phase into the pores of the UiO-66-X to the $H_2(vdW)$ and $CO_2(vdW)$ species is fast and is at equilibrium. We assume that the entropies of the vdW complexes are much smaller than the entropies of the gas-phase species, so that the change in entropy on going from the physisorbed to the transition states can be ignored. We further assume that the concentration of FA in the gas phase outside the MOF is kept low so that the reaction is irreversible. Although energetically unfavorable, we rationalize rapid desorption by noting the low diffusion barriers (Figure S11 in the Supporting Information) and entropic favorability for

DOI: 10.1021/acscatal.5b01191
ACS Catal. 2015, 5, 6219−6229

desorption of FA from the adsorbed phase to the gas phase. Additionally, our calculations indicate that FA can bind to the LP sites, but the most energetically favorable binding modes require that the FA rotate from the cis to the trans conformation. This rotational barrier is about 0.7 eV (Figure S12 in the Supporting Information), which is larger than the desorption energy. Details of how the Sabatier activities were computed are given in the Supporting Information. A contour plot of the Sabatier activity at 298 K is given in Figure 9. This

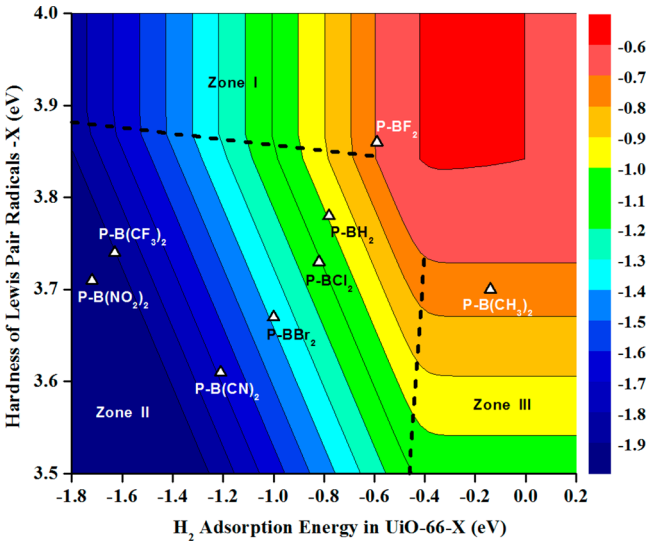

Figure 9. Contour plot of the Sabatier activity for the overall reaction rate for CO_2 hydrogenation at 298 K. The CO_2 hydrogenation barrier is given by a BEP relationship with the H_2 adsorption energy, and the H_2 dissociation barrier is given by a relationship with the hardness of the LP radicals -X. Specific LP groups are labeled on the figure.

analysis shows that UiO-66-P-BF_2 is closest to the top of the Sabatier activity contour but that it is not quite at the optimum location, denoted by the red region in Figure 9. The areas outside the optimal range, having lower Sabatier activities, can roughly be divided into three zones, as demarcated by the dashed lines in Figure 9. Zone I is characterized by large (negative) H_2 adsorption energies, giving rise to high barriers for CO_2 hydrogenation, which is therefore the rate-limiting step. In zone II the H_2 adsorption energies are large and the LP hardness values are small, so that both H_2 dissociation and CO_2 hydrogenation have high barriers. Zone III has low CO_2 hydrogenation barriers due to low H_2 adsorption energies but high H_2 dissociation barriers, making that the rate-limiting step. The Sabatier analysis indicates we should aim for functional groups having hardness in the range of about 3.8 and above and H_2 binding energies between about −0.45 and −0.1 eV. When the reaction energy is changed to 400 K, the results are qualitatively similar to those of Figure 9, as can be seen from Figure S14 in the Supporting Information.

The linear relationships between the H_2 adsorption energies on the LP functional groups X in the gas phase and the CO_2 hydrogenation barriers in UiO-66-X and also the correlation for ΔG_{ha} shown in Figure 7 provide the potential to make two more Sabatier contour plots, similar to that of Figure 9. These are shown in Figures S15 and S16 in the Supporting Information and show the same qualitative trends as Figure 9, but with some differences for the location of individual UiO-66-X materials.

One of the assumptions made in developing the model for the Sabatier activity was that the entropy change from the physisorbed state to the transition state is negligible. This is obviously not an accurate assumption. The opposite extreme is to assume that there is no entropy change in going from the gas phase to the physisorbed phase and that the entropy of the transition state species is 0 in comparison with the gas phase. This is more drastic than the assumption that the adsorbed and transition states have about the same entropy because H_2(vdW) and CO_2(vdW) are in highly confined environments with very little translational entropy and, for CO_2, reduced rotational entropy. Nevertheless, Sabatier activity calculations using the gas-phase entropy of H_2 and CO_2 produce contour plots that are similar to that of Figure 9, as can be seen from Figure S17 in the Supporting Information. This indicates that the trends predicted using either assumption are qualitatively similar, although the rates using the second assumption are much lower.

4. CONCLUSION

We have used DFT to computationally evaluate eight different Lewis pair (LP) moieties as catalysts for CO_2 hydrogenation in functionalized UiO-66. The reaction of CO_2 with H_2 in the UiO-66-X materials always proceeds by a two-step mechanism, with the first step being heterolytic dissociation of H_2 on the LP. The second step is a two-electron reduction accomplished by concerted addition of a hydride and a proton to CO_2, producing FA. The reaction barriers for H_2 dissociation range from 0.48 to 1.09 eV; the barriers for CO_2 hydrogenation fall between 0.28 and 1.79 eV. We note that the functionalized MOFs we propose in this work could likely be synthesized in a way similar to that proposed for UiO-66-P-BF_2.[36]

Brønsted−Evans−Polanyi relationships are powerful tools for predicting reaction barriers using surrogate quantities that can be more easily calculated. More importantly, they provide physical insight into properties controlling the reaction. While these BEP relationships have been identified for many reactions on metallic surfaces, to the best of our knowledge only two other BEP relationships have been identified for catalytic porous materials.[116,117] Our calculations have identified two BEP relationships for the reactions involving CO_2 hydrogenation in functionalized UiO-66, one relating to the barrier for concerted addition of a hydride and proton to CO_2 and another BEP relation for the recombination of the hydride and proton to produce H_2. The BEP relationship for CO_2 hydrogenation also applies to H_2 adsorption energies computed on the gas-phase functional moieties, in the absence of the UiO-66 framework. Furthermore, since the H_2 adsorption energies are linearly related to the hydride attachment energies, which are a measure of the acidity of the LP, we can correlate the CO_2 hydrogenation barriers in terms of the acidity of the gas-phase functional groups, as measured by the hydride attachment energy. These correlations provide an efficient method for screening potential functional groups for their activity toward CO_2 hydrogenation.

Identifying an estimator for the H_2 dissociation barriers has proved more difficult. The H_2 dissociation barriers for most, but not all, of the functional groups scale linearly with the hardness and the electron acceptor−donor bond angle of the LP moieties. Combining these relationships and applying Sabatier analysis generate insight into how to optimize functional groups for maximizing the activity of the catalyst. More generally, we believe that the approach of using gas-phase

DOI: 10.1021/acscatal.5b01191
ACS Catal. 2015, 5, 6219−6229

moieties as surrogates for functional groups bound within MOFs to construct BEP relationships and other correlations for CO_2 hydrogenation barriers and H_2 dissociation barriers can be applied to other types of functional groups and is not limited to the class of LP groups considered in this work.

One drawback of the LP functional groups considered in this work is that CO_2 and H_2 may bind competitively to the LP sites. This would require that in practice one would have to first expose the catalyst to a gas stream of H_2 and then subsequently to a stream of CO_2 to avoid the competitive binding, as noted previously for P-BF_2 functionalized UiO-66.[36] Future work will focus on designing groups that selectively react with H_2 without binding CO_2 significantly.

The functional groups considered in this work were generated by modifying the R groups attached to the Lewis acid site. Additional control over catalytic activity can be obtained by modifying the Lewis base site, which will be the subject of future work.

The best functional groups identified in this work have barriers that are among the lowest reported in the literature for nonelectrolytic reduction of CO_2 with H_2.[118−124]

■ ASSOCIATED CONTENT

Supporting Information

The Supporting Information is available free of charge on the ACS Publications website at DOI: 10.1021/acscatal.5b01191.

Solvent effect calculations, structures of UiO-66-X and UiO-66-X with adsorbed H_2 or CO_2, structures of initial, transition, and final state geometries of the reactions and the corresponding CI-NEB pathway energies, data for various figures, linear energy relationships for activation energies of H_2 formation, Sabatier activity models, and contour graphs (PDF)

■ AUTHOR INFORMATION

Corresponding Author

*E-mail for J.K.J.: karlj@pitt.edu.

Notes

The authors declare no competing financial interest.

■ ACKNOWLEDGMENTS

We gratefully acknowledge support from the U.S. Department of Energy (Grant No. DE-FG02-10ER16165). The computations were performed at the University of Pittsburgh's Center for Simulation & Modeling and at the Extreme Science and Engineering Discovery Environment (XSEDE) under project TG-CHE140046.

■ REFERENCES

(1) Aresta, M., Carbon Dioxide: Utilization Options to Reduce its Accumulation in the Atmosphere. In *Carbon Dioxide as Chemical Feedstock*; Aresta, M., Ed.; Wiley-VCH: Weinheim, Germany, 2010; pp 1−13.

(2) Nataly Echevarria Huaman, R.; Xiu Jun, T. *Renewable Sustainable Energy Rev.* **2014**, *31*, 368−385.

(3) Benhelal, E.; Zahedi, G.; Shamsaei, E.; Bahadori, A. *J. Cleaner Prod.* **2013**, *51*, 142−161.

(4) Markewitz, P.; Kuckshinrichs, W.; Leitner, W.; Linssen, J.; Zapp, P.; Bongartz, R.; Schreiber, A.; Muller, T. E. *Energy Environ. Sci.* **2012**, *5*, 7281−7305.

(5) Li, L.; Zhao, N.; Wei, W.; Sun, Y. *Fuel* **2013**, *108*, 112−130.

(6) Aresta, M.; Dibenedetto, A. *Dalton Trans.* **2007**, 2975−2992.

(7) Olah, G. A.; Prakash, G. K. S.; Goeppert, A. *J. Am. Chem. Soc.* **2011**, *133*, 12881−12898.

(8) Schaub, T.; Paciello, R. A. *Angew. Chem., Int. Ed.* **2011**, *50*, 7278−7282.

(9) Dibenedetto, A.; Angelini, A.; Stufano, P. *J. Chem. Technol. Biotechnol.* **2014**, *89*, 334−353.

(10) Izumi, Y. *Coord. Chem. Rev.* **2013**, *257*, 171−186.

(11) Lim, R. J.; Xie, M. S.; Sk, M. A.; Lee, J. M.; Fisher, A.; Wang, X.; Lim, K. H. *Catal. Today* **2014**, *233*, 169−180.

(12) Lu, X.; Leung, D. Y. C.; Wang, H. Z.; Leung, M. K. H.; Xuan, J. *ChemElectroChem* **2014**, *1*, 836−849.

(13) Costentin, C.; Robert, M.; Saveant, J.-M. *Chem. Soc. Rev.* **2013**, *42*, 2423−2436.

(14) Appel, A. M.; Bercaw, J. E.; Bocarsly, A. B.; Dobbek, H.; DuBois, D. L.; Dupuis, M.; Ferry, J. G.; Fujita, E.; Hille, R.; Kenis, P. J. A.; Kerfeld, C. A.; Morris, R. H.; Peden, C. H. F.; Portis, A. R.; Ragsdale, S. W.; Rauchfuss, T. B.; Reek, J. N. H.; Seefeldt, L. C.; Thauer, R. K.; Waldrop, G. L. *Chem. Rev.* **2013**, *113*, 6621−6658.

(15) Ma, J.; Sun, N.; Zhang, X.; Zhao, N.; Xiao, F.; Wei, W.; Sun, Y. *Catal. Today* **2009**, *148*, 221−231.

(16) Qiao, J.; Liu, Y.; Hong, F.; Zhang, J. *Chem. Soc. Rev.* **2014**, *43*, 631−675.

(17) Hull, J. F.; Himeda, Y.; Wang, W.-H.; Hashiguchi, B.; Periana, R.; Szalda, D. J.; Muckerman, J. T.; Fujita, E. *Nat. Chem.* **2012**, *4*, 383−388.

(18) Agarwal, A. S.; Zhai, Y.; Hill, D.; Sridhar, N. *ChemSusChem* **2011**, *4*, 1301−1310.

(19) Rice, C.; Ha, R. I.; Masel, R. I.; Waszczuk, P.; Wieckowski, A.; Barnard, T. *J. Power Sources* **2002**, *111*, 83−89.

(20) Lu, X.; Leung, D. Y. C.; Wang, H.; Leung, M. K. H.; Xuan, J. *ChemElectroChem* **2014**, *1*, 836−849.

(21) Boddien, A.; Mellmann, D.; Gartner, F.; Jackstell, R.; Junge, H.; Dyson, P. J.; Laurenczy, G.; Ludwig, R.; Beller, M. *Science* **2011**, *333*, 1733−1736.

(22) Tanaka, R.; Yamashita, M.; Nozaki, K. *J. Am. Chem. Soc.* **2009**, *131*, 14168−14169.

(23) Federsel, C.; Jackstell, R.; Beller, M. *Angew. Chem.* **2010**, *122*, 6392−6395.

(24) Fellay, C.; Dyson, P. J.; Laurenczy, G. *Angew. Chem., Int. Ed.* **2008**, *47*, 3966−3968.

(25) Tanaka, R.; Yamashita, M.; Nozaki, K. *J. Am. Chem. Soc.* **2009**, *131*, 14168−14169.

(26) Grasemann, M.; Laurenczy, G. *Energy Environ. Sci.* **2012**, *5*, 8171−8181.

(27) Jessop, P. G.; Joó, F.; Tai, C.-C. *Coord. Chem. Rev.* **2004**, *248*, 2425−2442.

(28) Wang, W.; Wang, S.; Ma, X.; Gong, J. *Chem. Soc. Rev.* **2011**, *40*, 3703−3727.

(29) Himeda, Y. *Eur. J. Inorg. Chem.* **2007**, *2007*, 3927−3941.

(30) Preti, D.; Squarcialupi, S.; Fachinetti, G. *Angew. Chem.* **2010**, *122*, 2635−2638.

(31) Costa, J. S.; Gamez, P.; Black, C. A.; Roubeau, O.; Teat, S. J.; Reedijk, J. *Eur. J. Inorg. Chem.* **2008**, *2008*, 1551−1554.

(32) Zhang, X.; Llabrés i Xamena, F. X.; Corma, A. *J. Catal.* **2009**, *265*, 155−160.

(33) Horiuchi, Y.; Toyao, T.; Saito, M.; Mochizuki, K.; Iwata, M.; Higashimura, H.; Anpo, M.; Matsuoka, M. *J. Phys. Chem. C* **2012**, *116*, 20848−20853.

(34) Pullen, S.; Fei, H.; Orthaber, A.; Cohen, S. M.; Ott, S. *J. Am. Chem. Soc.* **2013**, *135*, 16997−17003.

(35) Toyao, T.; Miyahara, K.; Fujiwaki, M.; Kim, T.-H.; Dohshi, S.; Horiuchi, Y.; Matsuoka, M. *J. Phys. Chem. C* **2015**, *119*, 8131−8137.

(36) Ye, J.; Johnson, J. K. *ACS Catal.* **2015**, *5*, 2921−2928.

(37) Cavka, J. H.; Jakobsen, S.; Olsbye, U.; Guillou, N.; Lamberti, C.; Bordiga, S.; Lillerud, K. P. *J. Am. Chem. Soc.* **2008**, *130*, 13850−13851.

(38) Valenzano, L.; Civalleri, B.; Chavan, S.; Bordiga, S.; Nilsen, M. H.; Jakobsen, S.; Lillerud, K. P.; Lamberti, C. *Chem. Mater.* **2011**, *23*, 1700−1718.

DOI: 10.1021/acscatal.5b01191
ACS Catal. 2015, 5, 6219−6229

(39) Norskov, J. K.; Bligaard, T.; Rossmeisl, J.; Christensen, C. H. *Nat. Chem.* **2009**, *1*, 37−46.
(40) Greeley, J.; Mavrikakis, M. *Nat. Mater.* **2004**, *3*, 810−815.
(41) Baik, M.-H.; Friesner, R. A. *J. Phys. Chem. A* **2002**, *106*, 7407−7412.
(42) Tsai, C.; Chan, K.; Norskov, J. K.; Abild-Pedersen, F. *Catal. Sci. Technol.* **2015**, *5*, 246−253.
(43) Bronsted, J. N. *Chem. Rev.* **1928**, *5*, 231−338.
(44) Evans, M. G.; Polanyi, M. *Trans. Faraday Soc.* **1938**, *34*, 11−24.
(45) Abild-Pedersen, F.; Greeley, J.; Studt, F.; Rossmeisl, J.; Munter, T. R.; Moses, P. G.; Skúlason, E.; Bligaard, T.; Nørskov, J. K. *Phys. Rev. Lett.* **2007**, *99*, 016105.
(46) Studt, F.; Sharafutdinov, I.; Abild-Pedersen, F.; Elkjær, C. F.; Hummelshøj, J. S.; Dahl, S.; Chorkendorff, I.; Nørskov, J. K. *Nat. Chem.* **2014**, *6*, 320−324.
(47) Bligaard, T.; Nørskov, J. K.; Dahl, S.; Matthiesen, J.; Christensen, C. H.; Sehested, J. *J. Catal.* **2004**, *224*, 206−217.
(48) Falsig, H.; Hvolbæk, B.; Kristensen, I. S.; Jiang, T.; Bligaard, T.; Christensen, C. H.; Nørskov, J. K. *Angew. Chem., Int. Ed.* **2008**, *47*, 4835−4839.
(49) Dahl, S.; Logadottir, A.; Jacobsen, C. J. H.; Nørskov, J. K. *Appl. Catal., A* **2001**, *222*, 19−29.
(50) Jiang, T.; Mowbray, D. J.; Dobrin, S.; Falsig, H.; Hvolbæk, B.; Bligaard, T.; Nørskov, J. K. *J. Phys. Chem. C* **2009**, *113*, 10548−10553.
(51) Logadottir, A.; Rod, T. H.; Nørskov, J. K.; Hammer, B.; Dahl, S.; Jacobsen, C. J. H. *J. Catal.* **2001**, *197*, 229−231.
(52) Wang, S.; Vorotnikov, V.; Sutton, J. E.; Vlachos, D. G. *ACS Catal.* **2014**, *4*, 604−612.
(53) Liu, Z.-P.; Hu, P. *J. Chem. Phys.* **2001**, *114*, 8244−8247.
(54) Michaelides, A.; Liu, Z. P.; Zhang, C. J.; Alavi, A.; King, D. A.; Hu, P. *J. Am. Chem. Soc.* **2003**, *125*, 3704−3705.
(55) Courtemanche, M.-A.; Légaré, M.-A.; Maron, L.; Fontaine, F.-G. *J. Am. Chem. Soc.* **2013**, *135*, 9326−9329.
(56) Courtemanche, M.-A.; Larouche, J.; Légaré, M.-A.; Bi, W.; Maron, L.; Fontaine, F.-G. *Organometallics* **2013**, *32*, 6804−6811.
(57) Berkefeld, A.; Piers, W. E.; Parvez, M. *J. Am. Chem. Soc.* **2010**, *132*, 10660−10661.
(58) Courtemanche, M.-A.; Légaré, M.-A.; Maron, L.; Fontaine, F.-G. *J. Am. Chem. Soc.* **2014**, *136*, 10708−10717.
(59) Lim, C.-H.; Holder, A. M.; Hynes, J. T.; Musgrave, C. B. *Inorg. Chem.* **2013**, *52*, 10062−10066.
(60) Sgro, M. J.; Domer, J.; Stephan, D. W. *Chem. Commun.* **2012**, *48*, 7253−7255.
(61) Ménard, G.; Stephan, D. W. *J. Am. Chem. Soc.* **2010**, *132*, 1796−1797.
(62) Ashley, A. E.; O'Hare, D. *Top. Curr. Chem.* **2013**, *334*, 191−217.
(63) Ashley, A. E.; Thompson, A. L.; O'Hare, D. *Angew. Chem., Int. Ed.* **2009**, *48*, 9839−9843.
(64) Courtemanche, M.-A.; Pulis, A. P.; Rochette, E.; Legare, M.-A.; Stephan, D. W.; Fontaine, F.-G. *Chem. Commun.* **2015**, *51*, 9797−9800.
(65) Mahdi, T.; Stephan, D. W. *J. Am. Chem. Soc.* **2014**, *136*, 15809−15812.
(66) Stephan, D. W.; Erker, G. *Angew. Chem., Int. Ed.* **2010**, *49*, 46−76.
(67) Whittemore, S. M.; Edvenson, G.; Camaioni, D. M.; Karkamkar, A.; Neiner, D.; Parab, K.; Autrey, T. *Catal. Today* **2015**, *251*, 28−33.
(68) Pu, M.; Privalov, T. *Inorg. Chem.* **2014**, *53*, 4598−4609.
(69) Mömming, C. M.; Otten, E.; Kehr, G.; Fröhlich, R.; Grimme, S.; Stephan, D. W.; Erker, G. *Angew. Chem., Int. Ed.* **2009**, *48*, 6643−6646.
(70) Rokob, T. A.; Hamza, A.; Pápai, I. *J. Am. Chem. Soc.* **2009**, *131*, 10701−10710.
(71) Rokob, T. A.; Hamza, A.; Stirling, A.; Soós, T.; Pápai, I. *Angew. Chem., Int. Ed.* **2008**, *47*, 2435−2438.
(72) Geier, S. J.; Stephan, D. W. *J. Am. Chem. Soc.* **2009**, *131*, 3476−3477.
(73) Welch, G. C.; Stephan, D. W. *J. Am. Chem. Soc.* **2007**, *129*, 1880−1881.
(74) Nyhlen, J.; Privalov, T. *Dalton Trans.* **2009**, 5780−5786.
(75) Rokob, T. A.; Hamza, A.; Stirling, A.; Pápai, I. *J. Am. Chem. Soc.* **2009**, *131*, 2029−2036.
(76) Camaioni, D. M.; Ginovska-Pangovska, B.; Schenter, G. K.; Kathmann, S. M.; Autrey, T. *J. Phys. Chem. A* **2012**, *116*, 7228−7237.
(77) Wang, Z.; Lu, G.; Li, H.; Zhao, L. *Chin. Sci. Bull.* **2010**, *55*, 239−245.
(78) Lu, G.; Li, H.; Zhao, L.; Huang, F.; Wang, Z.-X. *Inorg. Chem.* **2010**, *49*, 295−301.
(79) Sumerin, V.; Schulz, F.; Nieger, M.; Atsumi, M.; Wang, C.; Leskelä, M.; Pyykkö, P.; Repo, T.; Rieger, B. *J. Organomet. Chem.* **2009**, *694*, 2654−2660.
(80) Ullrich, M.; Lough, A. J.; Stephan, D. W. *J. Am. Chem. Soc.* **2009**, *131*, 52−53.
(81) Travis, A. L.; Binding, S. C.; Zaher, H.; Arnold, T. A. Q.; Buffet, J.-C.; O'Hare, D. *Dalton Trans.* **2013**, *42*, 2431−2437.
(82) Sabatier, P. *Ber. Dtsch. Chem. Ges.* **1911**, *44*, 1984−2001.
(83) VandeVondele, J.; Krack, M.; Mohamed, F.; Parrinello, M.; Chassaing, T.; Hutter, J. *Comput. Phys. Commun.* **2005**, *167*, 103−128.
(84) Grimme, S.; Antony, J.; Ehrlich, S.; Krieg, H. *J. Chem. Phys.* **2010**, *132*, 154104.
(85) Perdew, J. P.; Burke, K.; Ernzerhof, M. *Phys. Rev. Lett.* **1996**, *77*, 3865−3868.
(86) Goedecker, S.; Teter, M.; Hutter, J. *Phys. Rev. B: Condens. Matter Mater. Phys.* **1996**, *54*, 1703−1710.
(87) Henkelman, G.; Uberuaga, B. P.; Jónsson, H. *J. Chem. Phys.* **2000**, *113*, 9901−9904.
(88) Frisch, M. J.; Trucks, G. W.; Schlegel, H. B.; Scuseria, G. E.; Robb, M. A.; Cheeseman, J. R.; Scalmani, G.; Barone, V.; Mennucci, B.; Petersson, G. A.; Nakatsuji, H.; Caricato, M.; Li, X.; Hratchian, H. P.; Izmaylov, A. F.; Bloino, J.; Zheng, G.; Sonnenberg, J. L.; Hada, M.; Ehara, M.; Toyota, K.; Fukuda, R.; Hasegawa, J.; Ishida, M.; Nakajima, T.; Honda, Y.; Kitao, O.; Nakai, H.; Vreven, T.; Montgomery, J. A., Jr.; Peralta, J. E.; Ogliaro, F.; Bearpark, M. J.; Heyd, J.; Brothers, E. N.; Kudin, K. N.; Staroverov, V. N.; Kobayashi, R.; Normand, J.; Raghavachari, K.; Rendell, A. P.; Burant, J. C.; Iyengar, S. S.; Tomasi, J.; Cossi, M.; Rega, N.; Millam, N. J.; Klene, M.; Knox, J. E.; Cross, J. B.; Bakken, V.; Adamo, C.; Jaramillo, J.; Gomperts, R.; Stratmann, R. E.; Yazyev, O.; Austin, A. J.; Cammi, R.; Pomelli, C.; Ochterski, J. W.; Martin, R. L.; Morokuma, K.; Zakrzewski, V. G.; Voth, G. A.; Salvador, P.; Dannenberg, J. J.; Dapprich, S.; Daniels, A. D.; Farkas, Ö.; Foresman, J. B.; Ortiz, J. V.; Cioslowski, J.; Fox, D. J. *Gaussian 09*; Gaussian, Inc., Wallingford, CT, USA, 2009.
(89) Zhao, Y.; Truhlar, D. *Theor. Chem. Acc.* **2008**, *120*, 215−241.
(90) Rokob, T. A.; Pápai, I., Hydrogen activation by frustrated Lewis pairs: Insights from computational studies. In *Frustrated Lewis Pairs I*; Springer: Berlin, 2013; pp 157−211.
(91) De Proft, F.; Langenaeker, W.; Geerlings, P. *J. Phys. Chem.* **1993**, *97*, 1826−1831.
(92) Mulliken, R. S. *J. Chem. Phys.* **1934**, *2*, 782−793.
(93) Parr, R. G.; Donnelly, R. A.; Levy, M.; Palke, W. E. *J. Chem. Phys.* **1978**, *68*, 3801−3807.
(94) Parr, R. G.; Pearson, R. G. *J. Am. Chem. Soc.* **1983**, *105*, 7512−7516.
(95) Biswas, S.; Zhang, J.; Li, Z.; Liu, Y.-Y.; Grzywa, M.; Sun, L.; Volkmer, D.; Van Der Voort, P. *Dalton Trans.* **2013**, *42*, 4730−4737.
(96) Garibay, S. J.; Cohen, S. M. *Chem. Commun.* **2010**, *46*, 7700−7702.
(97) Kim, M.; Cohen, S. M. *CrystEngComm* **2012**, *14*, 4096−4104.
(98) Luan, Y.; Zheng, N. N.; Qi, Y.; Yu, J.; Wang, G. *Eur. J. Inorg. Chem.* **2014**, *2014*, 4268−4272.
(99) Vermoortele, F.; Bueken, B.; Le Bars, G.; Van de Voorde, B.; Vandichel, M.; Houthoofd, K.; Vimont, A.; Daturi, M.; Waroquier, M.; Van Speybroeck, V.; Kirschhock, C.; De Vos, D. E. *J. Am. Chem. Soc.* **2013**, *135*, 11465−11468.
(100) Wang, C.; deKrafft, K. E.; Lin, W. *J. Am. Chem. Soc.* **2012**, *134*, 7211−7214.
(101) Wang, C.; Xie, Z.; deKrafft, K. E.; Lin, W. *J. Am. Chem. Soc.* **2011**, *133*, 13445−13454.

DOI: 10.1021/acscatal.5b01191
ACS Catal. 2015, 5, 6219−6229

(102) Kim, M.; Cahill, J. F.; Su, Y.; Prather, K. A.; Cohen, S. M. *Chem. Sci.* **2012**, *3*, 126−130.
(103) Cohen, S. M. *Chem. Rev.* **2012**, *112*, 970−1000.
(104) Wang, Z.; Cohen, S. M. *Chem. Soc. Rev.* **2009**, *38*, 1315−1329.
(105) Biswas, S.; Van Der Voort, P. *Eur. J. Inorg. Chem.* **2013**, *2013*, 2154−2160.
(106) Zlotea, C.; Phanon, D.; Mazaj, M.; Heurtaux, D.; Guillerm, V.; Serre, C.; Horcajada, P.; Devic, T.; Magnier, E.; Cuevas, F.; Ferey, G.; Llewellyn, P. L.; Latroche, M. *Dalton Trans.* **2011**, *40*, 4879−4881.
(107) Yang, Q.; Wiersum, A. D.; Llewellyn, P. L.; Guillerm, V.; Serre, C.; Maurin, G. *Chem. Commun.* **2011**, *47*, 9603−9605.
(108) Huang, Y.; Qin, W.; Li, Z.; Li, Y. *Dalton Trans.* **2012**, *41*, 9283−9285.
(109) Cmarik, G. E.; Kim, M.; Cohen, S. M.; Walton, K. S. *Langmuir* **2012**, *28*, 15606−15613.
(110) Abid, H. R.; Tian, H.; Ang, H.-M.; Tade, M. O.; Buckley, C. E.; Wang, S. *Chem. Eng. J.* **2012**, *187*, 415−420.
(111) Chavan, S.; Vitillo, J. G.; Gianolio, D.; Zavorotynska, O.; Civalleri, B.; Jakobsen, S.; Nilsen, M. H.; Valenzano, L.; Lamberti, C.; Lillerud, K. P.; Bordiga, S. *Phys. Chem. Chem. Phys.* **2012**, *14*, 1614−1626.
(112) Zimmerman, P. M.; Zhang, Z.; Musgrave, C. B. *Inorg. Chem.* **2010**, *49*, 8724−8728.
(113) Pearson, R. G. *J. Am. Chem. Soc.* **1963**, *85*, 3533−3539.
(114) Pearson, R. G. *Science* **1966**, *151*, 172−177.
(115) Nørskov, J. K.; Bligaard, T.; Logadottir, A.; Bahn, S.; Hansen, L. B.; Bollinger, M.; Bengaard, H.; Hammer, B.; Sljivancanin, Z.; Mavrikakis, M.; Xu, Y.; Dahl, S.; Jacobsen, C. J. H. *J. Catal.* **2002**, *209*, 275−278.
(116) Joshi, Y. V.; Thomson, K. T. *J. Catal.* **2007**, *246*, 249−265.
(117) Silaghi, M.-C.; Chizallet, C.; Petracovschi, E.; Kerber, T.; Sauer, J.; Raybaud, P. *ACS Catal.* **2015**, *5*, 11−15.
(118) Peng, G.; Sibener, S. J.; Schatz, G. C.; Mavrikakis, M. *Surf. Sci.* **2012**, *606*, 1050−1055.
(119) Vesselli, E.; Rizzi, M.; De Rogatis, L.; Ding, X.; Baraldi, A.; Comelli, G.; Savio, L.; Vattuone, L.; Rocca, M.; Fornasiero, P.; Baldereschi, A.; Peressi, M. *J. Phys. Chem. Lett.* **2010**, *1*, 402−406.
(120) Grabow, L. C.; Mavrikakis, M. *ACS Catal.* **2011**, *1*, 365−384.
(121) Zhao, Y.-F.; Yang, Y.; Mims, C.; Peden, C. H. F.; Li, J.; Mei, D. *J. Catal.* **2011**, *281*, 199−211.
(122) Ye, J.; Liu, C.-j.; Mei, D.; Ge, Q. *J. Catal.* **2014**, *317*, 44−53.
(123) Ye, J.; Liu, C.; Ge, Q. *J. Phys. Chem. C* **2012**, *116*, 7817−7825.
(124) Liu, C.; Yang, B.; Tyo, E.; Seifert, S.; DeBartolo, J.; von Issendorff, B.; Zapol, P.; Vajda, S.; Curtiss, L. A. *J. Am. Chem. Soc.* **2015**, *137*, 8676−8679.

DOI: 10.1021/acscatal.5b01191
ACS Catal. 2015, 5, 6219−6229